



Exploring the Kinematics and Kinetics of the novel CT-3RPRS Robot

Oveas Gholami, Behnam Miripour Fard * 

Faculty of Mechanical Engineering, University of Guilan, Rasht, Iran.

ABSTRACT: This paper comprehensively investigates the dynamic modeling and simulation of the conjoined twins 3RPRS (CT-3RPRS) robot, an advanced parallel spatial mechanism distinguished by its kinematic efficiency, structural rigidity, and expansive accessible workspace. The CT-3RPRS robot is equipped with six actuators, comprising three prismatic and three revolute actuators, which contribute to its unique structure, enabling precise control over its constrained kinematic chains. To thoroughly analyze the robot's kinematics and kinetics, the Jacobian matrix and Lagrange multipliers are employed, respectively, to resolve reaction forces and moments inherent to closed-loop topologies. Motion equations are systematically derived using dual methodologies: the Euler-Lagrange formulation, which accounts for energy-based dynamics, and the principle of virtual work, which ensures equilibrium under non-conservative forces. These equations are subsequently verified to ensure their equivalence. The comprehensive modeling processes are rigorously validated through MATLAB simulations, providing a robust framework for analysis. Additionally, the results obtained from MATLAB are corroborated using SimScape, further confirming the accuracy and reliability of the dynamic models. This study highlights the dynamic features of the CT-3RPRS robot as well as the effectiveness of the employed modeling techniques.

Review History:

Received: Oct. 30, 2024

Revised: Mar. 08, 2025

Accepted: Mar. 28, 2025

Available Online: Mar. 31, 2025

Keywords:

Conjoined-Twins Parallel Robot

CT-3RPRS

Kinematics

Dynamics

Simulation

1- Introduction

Parallel robots have gained significant popularity in industrial applications due to their favorable payload-to-weight ratio and superior accuracy and repeatability compared to serial robots [1]. Continuous research efforts focus on enhancing the kinematic and dynamic aspects of these robots, as well as exploring new parallel robot structures.

The concept of Conjoined-Twins (CT) for parallel robots was recently introduced by Gholami and Miripour Fard [2, 3]. The recently introduced Conjoined-Twins-3RPRS (CT-3RPRS) parallel robot presents a structural modification of the 3RPRS robot, aimed at expanding its reachable workspace [3]. Kinematic analysis of the CT-3RPRS robot revealed promising results, demonstrating a larger workspace and improved maneuverability. However, its dynamic behavior remains unexplored.

This paper addresses the dynamic analysis of the CT-3RPRS robot. Given the novelty of this robot and the absence of prior research on its dynamics, a review of the 3RPRS robot's research background is crucial.

Previous studies [4-7] primarily focused on the kinematics of the 3RPRS robot and its variations. In 2009, Simas et al. conducted kinematic modeling of the Eclipse

and Eclipse II robots as a basis for the 3RPRS robot using an analytical approach [6], and investigated their singularities. The method introduced and employed by them was based on the concept of virtual chains. In 2014, Venkatesan et al. performed inverse kinematic modeling of the 3RPRS robot [7] and validated their results through simulations in the ADAMS software environment. In 2017, Nag et al. analyzed the forward kinematics of the 3RPRS robot and proposed a closed-loop solution for it [5]. Finally, Kumar and Bandyopadhyay addressed the forward kinematic modeling of the aforementioned robot using a geometric approach [4], providing both analytical and numerical solutions.

The only research on the 3RPRS robot's dynamics was conducted by Mohan and Corves [8], where they derived the dynamic equations using the Euler-Lagrange method, employing six generalized coordinates of the end-effector and incorporating system constraints in the kinematic modeling. Additionally, numerous studies have been conducted on similar parallel robots, some of which are highlighted below. Li and Xu investigated the 3RPRS robot [9], deriving the kinematic equations of the 3RPRS mechanism. They obtained an exact solution for the inverse kinematics and a numerical solution for the forward kinematics. Furthermore, they analyzed the dynamic equations using both the Euler-Lagrange method and the principle of virtual work, with

*Corresponding author's email: bmf@guilan.ac.ir



a focus on inverse dynamics. Building on this work, Pond and Carretero explored the structural optimization of the 3PRS robot [10]. Subsequently, Staicu examined the 3PRS mechanism [11], deriving the equations of motion using the Euler-Lagrange method and expressing them in matrix form. The results were validated using the principle of virtual work. Staicu also solved the inverse dynamics of the mechanism and calculated the required actuator forces. More recently, Tourajizadeh and Gholami focused on the modeling and optimal control of the 3PRS robot, utilizing the Euler-Lagrange method and the State-Dependent Riccati Equation (SDRE) approach for this purpose [12].

This study presents the first comprehensive dynamic analysis of the recently introduced Conjoined-Twins-3RPRS (CT-3RPRS) parallel robot, addressing a significant gap in the literature. While previous research has focused on the kinematic advantages of the CT-3RPRS robot, such as its expanded workspace and improved maneuverability, its dynamic behavior remains unexplored. To bridge this gap, the dynamic equations of the CT-3RPRS robot are derived using two distinct methodologies: the Euler-Lagrange method, providing a standard matrix form of the equations, and the principle of virtual work, chosen for its simplicity and accessibility. The kinematic modeling is systematically conducted using the Denavit-Hartenberg (DH) convention, and the Jacobian formulation is extracted to facilitate motion analysis. Furthermore, the system's constraint equations are incorporated into the kinematic and kinetic modeling to ensure accuracy. The validity of the proposed models is

confirmed through comparative simulations in MATLAB and SimScape, demonstrating their reliability. By providing a robust dynamic framework for the CT-3RPRS robot, this study lays the groundwork for advanced control strategies, such as optimal control and trajectory planning. It contributes to the broader understanding of novel parallel robot structures.

The paper is structured as follows: Section two presents a detailed representation of the robot's modeling, encompassing both kinematics and kinetics. Section three validates the modeling through numerical and comparative simulation scenarios conducted in MATLAB and SimScape. Finally, concluding remarks are provided in section four.

2- CT-3RPRS parallel robot

This section presents a kinematic and kinetic model of the Conjoined Twins 3RPRS (CT-3RPRS) robot, an innovative parallel mechanism consisting of two interconnected 3RPRS robots shown in Fig. 1. This 6 DOF robot utilizes three prismatic and three rotary actuators situated within its middle plane. The robot's kinematic structure comprises nine revolute, six spherical, and three prismatic joints.

2- 1- Kinematic modeling:

The kinematics of the CT-3RPRS robot is given in [3] and a summary of it is reviewed here:

2- 1- 1- Position:

Point **Q** is in the center of the end-effector and the goal is to calculate its position. Global coordinates origin is the **O** point and the i^{th} base spherical joint position is the A_i point (Fig 1).

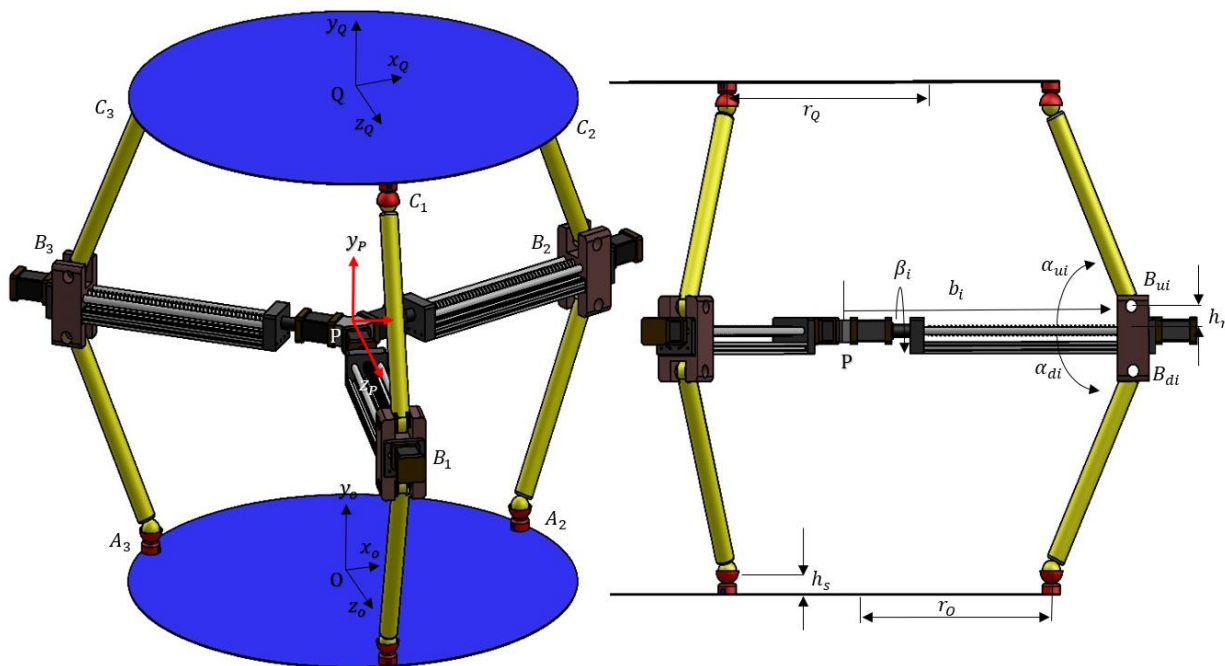


Fig. 1. CT-3RPRS robot structure [3]

Therefore, it can be written as follows:

$$\mathbf{O} = \begin{bmatrix} 0 \\ 0 \\ 0 \end{bmatrix}, \mathbf{A}_1 = \begin{bmatrix} 0 \\ h_s \\ r_o \end{bmatrix}, \quad (1)$$

$$\mathbf{A}_2 = \frac{1}{2} \begin{bmatrix} r_o \sqrt{3} \\ h_s \\ -r_o \end{bmatrix}, \mathbf{A}_3 = \frac{1}{2} \begin{bmatrix} -r_o \sqrt{3} \\ h_s \\ -r_o \end{bmatrix}$$

where h_s and r_o are the base plane radius and the spherical joint distance to the connected part, respectively. The end-effector angles in the global coordinate are considered as the yaw-pitch-roll (Euler angles). Therefore, the rotation matrix can be written as follows:

$$\mathbf{R}_Q^O = \mathbf{R}_{z, \varphi_Q} \mathbf{R}_{y, \theta_Q} \mathbf{R}_{x, \psi_Q} = \begin{bmatrix} c\varphi_Q c\theta_Q & -s\varphi_Q c\psi_Q & s\varphi_Q s\psi_Q \\ c\varphi_Q s\theta_Q & +c\varphi_Q s\theta_Q s\psi_Q & +c\varphi_Q s\theta_Q c\psi_Q \\ s\varphi_Q c\theta_Q & c\varphi_Q c\psi_Q & -c\varphi_Q s\psi_Q \\ -s\theta_Q & +s\varphi_Q s\theta_Q s\psi_Q & +s\varphi_Q s\theta_Q c\psi_Q \\ -s\theta_Q & c\theta_Q s\psi_Q & c\theta_Q c\psi_Q \end{bmatrix} \quad (2)$$

The C_i joint position can be written as follows:

$$\begin{bmatrix} C_1^o & C_2^o & C_3^o \\ 1 & 1 & 1 \end{bmatrix} (x_Q, y_Q, z_Q, \psi_Q, \theta_Q, \varphi_Q) = \mathbf{H}_Q^o = \begin{bmatrix} 0 & \frac{r_o \sqrt{3}}{2} & -\frac{r_o \sqrt{3}}{2} \\ -h_s & -h_s & -h_s \\ r_o & -\frac{r_o}{2} & -\frac{r_o}{2} \\ 1 & 1 & 1 \end{bmatrix}, \quad (3)$$

$$\mathbf{H}_Q^o = \begin{bmatrix} \mathbf{R}_Q^o & \mathbf{Q} \\ [0]_{1 \times 3} & 1 \end{bmatrix}, \mathbf{Q} = \begin{bmatrix} x_Q \\ y_Q \\ z_Q \end{bmatrix}.$$

where r_o is the end-effector radius. To calculate the α_i angles, as shown in Fig. 2 can be written:

The links D-H parameters can be written as follows (Table 1):

Therefore, the homogeneous transfer matrix can be written as follows:

$$\mathbf{H}_{B_{u1}}^P = \begin{bmatrix} \sin(\beta_1) & 0 & \cos(\beta_1) & -h_r \sin(\beta_1) \\ -\cos(\beta_1) & 0 & \sin(\beta_1) & h_r \cos(\beta_1) \\ 0 & -1 & 0 & b_1 \\ 0 & 0 & 0 & 1 \end{bmatrix}, \quad (4)$$

$$\mathbf{H}_{B_{d1}}^P = \begin{bmatrix} -\sin(\beta_1) & 0 & -\cos(\beta_1) & h_r \sin(\beta_1) \\ \cos(\beta_1) & 0 & -\sin(\beta_1) & -h_r \cos(\beta_1) \\ 0 & -1 & 0 & b_1 \\ 0 & 0 & 0 & 1 \end{bmatrix}$$

Besides these relations, the other two links have a more rotation around the y-axis. Therefore, can be written as:

$$\mathbf{H}_{B_{u2}}^P = \begin{bmatrix} \frac{\sin(\beta_2)}{2} & -\frac{\sqrt{3}}{2} & -\frac{\cos(\beta_2)}{2} & \frac{\sqrt{3}}{2} b_2 + \frac{1}{2} h_r \sin(\beta_2) \\ -\cos(\beta_2) & 0 & \sin(\beta_2) & h_r \cos(\beta_2) \\ -\frac{\sqrt{3}}{2} \sin(\beta_2) & 0.5 & -\frac{\sqrt{3}}{2} \cos(\beta_2) & -\frac{1}{2} b_2 + \frac{\sqrt{3}}{2} h_r \sin(\beta_2) \\ 0 & 0 & 0 & 1 \end{bmatrix}$$

$$\mathbf{H}_{B_{d2}}^P = \begin{bmatrix} \frac{\sin(\beta_2)}{2} & -\frac{\sqrt{3}}{2} & \frac{\cos(\beta_2)}{2} & \frac{\sqrt{3}}{2} b_2 - \frac{1}{2} h_r \sin(\beta_2) \\ \cos(\beta_2) & 0 & -\sin(\beta_2) & -h_r \cos(\beta_2) \\ \frac{\sqrt{3}}{2} \sin(\beta_2) & 0.5 & \frac{\sqrt{3}}{2} \cos(\beta_2) & -\frac{1}{2} b_2 - \frac{\sqrt{3}}{2} h_r \sin(\beta_2) \\ 0 & 0 & 0 & 1 \end{bmatrix}$$

$$\mathbf{H}_{B_{u3}}^P = \begin{bmatrix} -\frac{\sin(\beta_3)}{2} & \frac{\sqrt{3}}{2} & -\frac{\cos(\beta_3)}{2} & -\frac{\sqrt{3}}{2} b_3 + \frac{1}{2} h_r \sin(\beta_3) \\ -\cos(\beta_3) & 0 & \sin(\beta_3) & h_r \cos(\beta_3) \\ \frac{\sqrt{3}}{2} \sin(\beta_3) & 0.5 & \frac{\sqrt{3}}{2} \cos(\beta_3) & -\frac{\sqrt{3}}{2} h_r \sin(\beta_3) \\ 0 & 0 & 0 & 1 \end{bmatrix}, \quad (5)$$

$$\mathbf{H}_{B_{d3}}^P = \begin{bmatrix} \frac{\sin(\beta_3)}{2} & \frac{\sqrt{3}}{2} & \frac{\cos(\beta_3)}{2} & -\frac{\sqrt{3}}{2} b_3 + \frac{1}{2} h_r \sin(\beta_3) \\ \cos(\beta_3) & 0 & -\sin(\beta_3) & -h_r \cos(\beta_3) \\ -\frac{\sqrt{3}}{2} \sin(\beta_3) & 0.5 & -\frac{\sqrt{3}}{2} \cos(\beta_3) & +\frac{\sqrt{3}}{2} h_r \sin(\beta_3) \\ 0 & 0 & 0 & 1 \end{bmatrix}$$

The C_i and A_i joint's local positions can be written as:

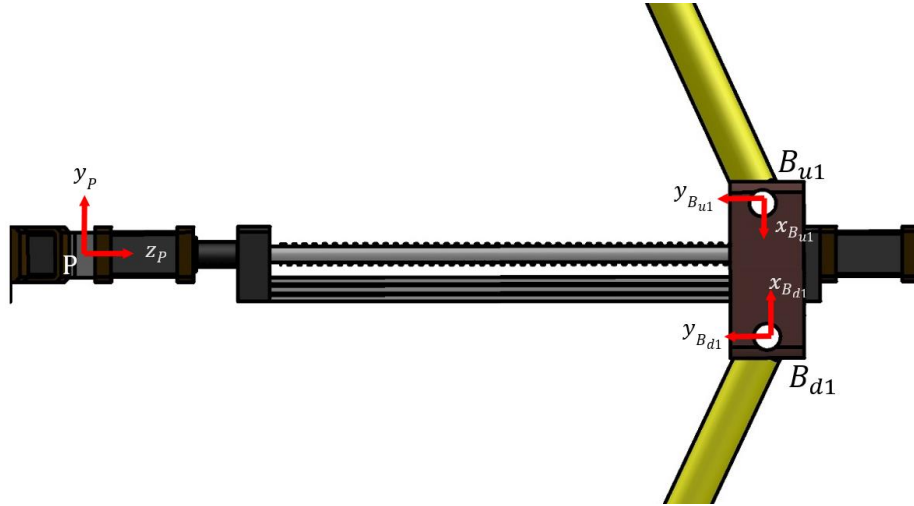


Fig. 2. Schematic of the local coordinates [3]

Table 1. Parameters of the Denavit-Hartenberg convention [3]

Link	e	γ	d	Θ
PB _{u1}	-h _r	-90	b ₁	$\beta_1 - 90$
PB _{d1}	-h _r	-90	b ₁	$\beta_1 + 90$

$$C_i^{B_{ui}} = l_u \begin{bmatrix} -\sin \alpha_{ui} \\ \cos \alpha_{ui} \\ 0 \end{bmatrix}, \quad A_i^{B_{di}} = l_d \begin{bmatrix} -\sin \alpha_{di} \\ \cos \alpha_{di} \\ 0 \end{bmatrix} \quad (6)$$

where l_u and l_d are the link lengths. Also, α_{ui} and α_{di} are the link angles with their carrier rails. The actuator plane angles were considered as the yaw-pitch-roll (Euler angles). Therefore, the transformation matrix can be written as:

$$H_P^O = \begin{bmatrix} R_P^O & P \\ [0]_{1 \times 3} & 1 \end{bmatrix}, \quad P = \begin{bmatrix} x_P \\ y_P \\ z_P \end{bmatrix} \quad (7)$$

Global positions of the C_i and A_i joints can be written as:

$$\left\{ \begin{array}{l} \begin{bmatrix} C_i^O \\ 1 \end{bmatrix} (x_P, y_P, z_P, \psi_P, \theta_P, \varphi_P, \beta_1, \beta_2, \beta_3, b_1, b_2, b_3, \alpha_{u1}, \alpha_{u2}, \alpha_{u3}) = \\ H_P^O H_{B_{ui}}^P \begin{bmatrix} C_i^{B_{ui}} \\ 1 \end{bmatrix} \\ \\ \begin{bmatrix} A_i^O \\ 1 \end{bmatrix} (x_P, y_P, z_P, \psi_P, \theta_P, \varphi_P, \beta_1, \beta_2, \beta_3, b_1, b_2, b_3, \alpha_{d1}, \alpha_{d2}, \alpha_{d3}) = \\ H_P^O H_{B_{di}}^P \begin{bmatrix} A_i^{B_{di}} \\ 1 \end{bmatrix} \end{array} \right. , \quad i = 1, 2, 3. \quad (8)$$

Using Eqs. (1, 3, and 8), the constraints can be written as:

$$f_{18 \times 1} = \begin{bmatrix} A_1^O \\ A_2^O \\ A_3^O \\ C_1^O \\ C_2^O \\ C_3^O \end{bmatrix} (x_P, y_P, z_P, \psi_P, \theta_P, \varphi_P, \beta_1, \beta_2, \beta_3, b_1, b_2, b_3, \alpha_{u1}, \alpha_{u2}, \alpha_{u3}, \alpha_{d1}, \alpha_{d2}, \alpha_{d3}) = 0 \quad (9)$$

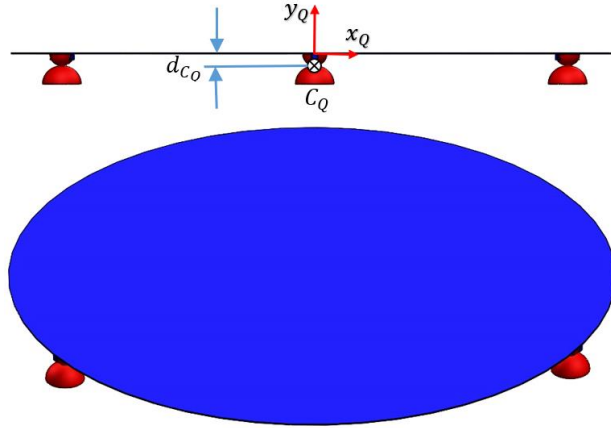


Fig. 3. The position of the platform and spherical joints and their center of mass

2- 1- 2- Velocity

By using the constraints equation, the Jacobian matrix can be written as [3]:

The velocity relationship of the end-effector coordinates and active joints can be written as:

$$\begin{cases} \frac{d}{dt} \mathbf{f}_{18 \times 1} = \frac{\partial \mathbf{f}}{\partial \bar{\mathbf{X}}} \dot{\bar{\mathbf{X}}} = 0 \\ \bar{\mathbf{X}}_{24 \times 1} = \begin{bmatrix} x_Q, y_Q, z_Q, \psi_Q, \theta_Q, \phi_Q, \dots \\ x_P, y_P, z_P, \psi_P, \theta_P, \phi_P, \dots \\ \alpha_{u1}, \alpha_{u2}, \alpha_{u3}, \alpha_{d1}, \alpha_{d2}, \dots \\ \alpha_{d3}, \beta_1, \beta_2, \beta_3, b_1, b_2, b_3 \end{bmatrix}^T \end{cases} \quad (10)$$

$$\begin{bmatrix} \dot{x}_Q \\ \dot{y}_Q \\ \dot{z}_Q \\ \dot{\psi}_Q \\ \dot{\theta}_Q \\ \dot{\phi}_Q \end{bmatrix} = \mathbf{J}(1:6,:) |_{6 \times 6} \begin{bmatrix} \dot{\beta}_1 \\ \dot{\beta}_1 \\ \dot{\beta}_3 \\ \dot{b}_1 \\ \dot{b}_1 \\ \dot{b}_3 \end{bmatrix} \quad (13)$$

By a detailed description of equation 10 we have:

2- 2- Dynamics modeling:

2- 2- 1- Euler-Lagrange method

$$\frac{\partial \mathbf{f}}{\partial \bar{\mathbf{X}}} \dot{\bar{\mathbf{X}}} = 0 \rightarrow \mathbf{J}_p \dot{\bar{\mathbf{X}}}_p + \mathbf{J}_a \dot{\bar{\mathbf{X}}}_a = 0 \rightarrow \dot{\bar{\mathbf{X}}}_p = -\mathbf{J}_p^{-1} \mathbf{J}_a \dot{\bar{\mathbf{X}}}_a$$

$$\begin{bmatrix} x_Q, y_Q, z_Q, \psi_Q, \theta_Q, \phi_Q, x_P, y_P, z_P, \psi_P, \theta_P, \phi_P, \\ \alpha_{u1}, \alpha_{u2}, \alpha_{u3}, \alpha_{d1}, \alpha_{d2}, \alpha_{d3}, \beta_1, \beta_2, \beta_3, b_1, b_2, b_3 \end{bmatrix}^T$$

$$\begin{cases} \mathbf{J}_p |_{18 \times 18} = \partial \mathbf{f} / \partial \bar{\mathbf{X}}_p, \quad \mathbf{J}_a |_{18 \times 6} = \partial \mathbf{f} / \partial \bar{\mathbf{X}}_a \\ \bar{\mathbf{X}}_a |_{6 \times 1} = [\beta_1, \beta_2, \beta_3, b_1, b_2, b_3]^T \\ \bar{\mathbf{X}}_p |_{18 \times 1} = [x_Q, y_Q, z_Q, \psi_Q, \theta_Q, \phi_Q, x_P, y_P, z_P, \psi_P, \theta_P, \phi_P, \alpha_{u1}, \alpha_{u2}, \alpha_{u3}, \alpha_{d1}, \alpha_{d2}, \alpha_{d3}]^T \end{cases} \quad (11)$$

is considered as twenty-four generalized coordinates. These coordinates have been defined in the kinematics section. The Euler-Lagrange method [13] was used to derive the equations of motion of the system. For this purpose, the inertia matrix and the linear and angular velocities of each component of the robot were calculated separately. As shown in Fig. 3, the robot platform with three spherical joints attached to it was considered as a set, and its inertia matrix was extracted.

where the passive and active abbreviation indexes are p and a . Eq. (11) can be written as follows:

The local coordinates \mathbf{Q} on the mass center of the platform were used to calculate the inertia matrix. To calculate \mathbf{I}_Q we can write:

$$\begin{cases} \dot{\bar{\mathbf{X}}}_p = \mathbf{J} |_{18 \times 6} \dot{\bar{\mathbf{X}}}_a \\ \mathbf{J} = -\mathbf{J}_p^{-1} \mathbf{J}_a \end{cases} \quad (12)$$

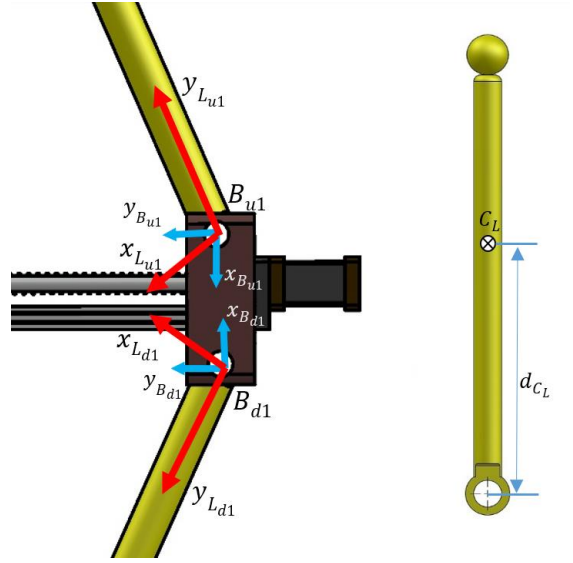


Fig. 4. Position of the center of mass and local coordinates of the links and joints

$$\mathbf{I}_Q = \mathbf{R}_Q^O \mathbf{I}_{Q_{Local}} \mathbf{R}_Q^{OT},$$

$$\mathbf{I}_{Q_{Local}} = \begin{bmatrix} 0.03 & 0 & 0 \\ 0 & 0.06 & 0.001 \\ 0 & 0.001 & 0.03 \end{bmatrix}. \quad (14)$$

According to Fig. 4, the moment of inertia of each link relative to its center of mass was written in the local coordinate system connected to the same link; and to transfer it to the reference coordinate system, the rotation matrix of these two coordinates relative to each other was used.

$$\begin{cases} \mathbf{I}_{L_{ui}} = \mathbf{R}_{L_{ui}}^O \mathbf{I}_{L_{ui}Local} \mathbf{R}_{L_{ui}}^{OT} \\ \mathbf{R}_{L_{ui}}^O = \mathbf{R}_P^O \mathbf{R}_{B_{ui}}^P \mathbf{R}_z, \alpha_{ui} \end{cases},$$

$$\begin{cases} \mathbf{I}_{L_{di}} = \mathbf{R}_{L_{di}}^O \mathbf{I}_{L_{di}Local} \mathbf{R}_{L_{di}}^{OT} \\ \mathbf{R}_{L_{di}}^O = \mathbf{R}_P^O \mathbf{R}_{B_{di}}^P \mathbf{R}_z, \alpha_{di} \end{cases}, \quad (15)$$

$$\mathbf{I}_{L_{i}Local} = \begin{bmatrix} 0.01 & 0 & 0 \\ 0 & 0 & 0 \\ 0 & 0 & 0.01 \end{bmatrix}.$$

As shown in Fig. 5, the robot actuators consist of three parts (including the rigid part BA , the rotary ones RA_i , and the slider part SA_i). To calculate the inertia matrix, the local coordinates of each component on its center of mass were used, and using the rotation matrices were taken to the reference coordinates.

So, we can write:

$$\begin{cases} \mathbf{I}_{RA_i} = \mathbf{R}_{RA_i}^O \mathbf{I}_{RA_{Local}} \mathbf{R}_{RA_i}^{OT} \\ \mathbf{R}_{RA_i}^O = \mathbf{R}_P^O \mathbf{R}_{RA_i}^P \end{cases}, \quad (16)$$

$$\begin{cases} \mathbf{I}_{SA_i} = \mathbf{R}_{SA_i}^O \mathbf{I}_{SA_{Local}} \mathbf{R}_{SA_i}^{OT} \\ \mathbf{I}_{BA} = \mathbf{R}_P^O \mathbf{I}_{BA_{Local}} \mathbf{R}_P^{OT} \end{cases}.$$

It should be noted that, due to the absence of relative rotation between the components RA_i and SA_i , the rotation matrix applicable to the component RA_i is equally valid for the component SA_i . Consequently, the local inertia matrix, as expressed in Equation 16, is given by:

$$\mathbf{I}_{BA_{Local}} = \begin{bmatrix} 0.001 & 0 & 0 \\ 0 & 0.001 & 0 \\ 0 & 0 & 0.001 \end{bmatrix},$$

$$\mathbf{I}_{RA_{Local}} = \begin{bmatrix} 0.001 & 0 & 0 \\ 0 & 0.001 & 0 \\ 0 & 0 & 0 \end{bmatrix}$$

$$\mathbf{I}_{SA_{Local}} = \begin{bmatrix} 0.005 & 0 & 0 \\ 0 & 0.005 & 0 \\ 0 & 0 & 0 \end{bmatrix} \quad (17)$$

As mentioned in the kinematics section, we derive the

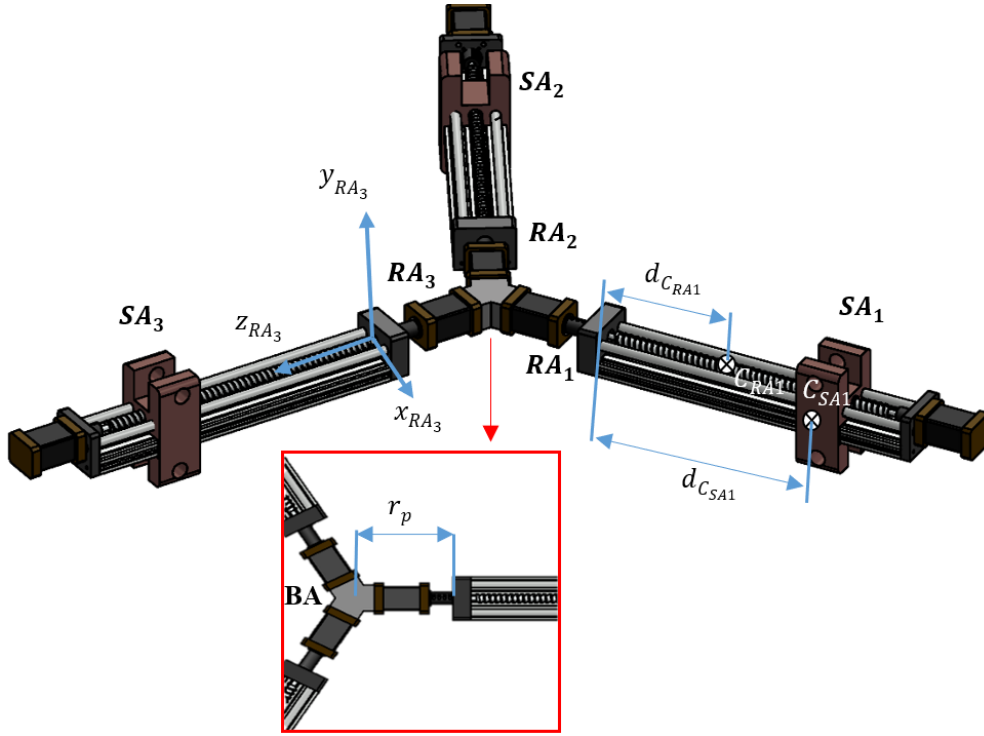


Fig. 5. Different parts of the actuator plane and the status of local coordinates and their center of mass

$\mathbf{H}_{RA_i}^P$, homogeneous transfer matrices using the Denavit–Hartenberg method.

In Table 2 r_p represents the radius of the BA component. The other two links are exactly the same as the first link, except that they have an extra rotation around the y -axis. The homogeneous transfer matrix, according to the parameters of Table 2 is as follows:

$$\mathbf{H}_{RA_1}^P = \begin{bmatrix} \cos(\beta_1) & -\sin(\beta_1) & 0 & 0 \\ \sin(\beta_1) & \cos(\beta_1) & 0 & 0 \\ 0 & 0 & 1 & r_p \\ 0 & 0 & 0 & 1 \end{bmatrix},$$

$$\mathbf{H}_{RA_2}^P = \begin{bmatrix} -\frac{1}{2}\cos(\beta_2) & \frac{1}{2}\sin(\beta_2) & \frac{\sqrt{3}}{2} & \frac{\sqrt{3}}{2}r_p \\ \sin(\beta_2) & \cos(\beta_2) & 0 & 0 \\ -\frac{\sqrt{3}}{2}\cos(\beta_2) & \frac{\sqrt{3}}{2}\sin(\beta_2) & -\frac{1}{2} & -\frac{1}{2}r_p \\ 0 & 0 & 0 & 1 \end{bmatrix},$$

$$\mathbf{H}_{RA_3}^P = \begin{bmatrix} -\frac{1}{2}\cos(\beta_3) & \frac{1}{2}\sin(\beta_3) & -\frac{\sqrt{3}}{2} & -\frac{\sqrt{3}}{2}r_p \\ \sin(\beta_3) & \cos(\beta_3) & 0 & 0 \\ \frac{\sqrt{3}}{2}\cos(\beta_3) & -\frac{\sqrt{3}}{2}\sin(\beta_3) & \frac{1}{2} & \frac{1}{2}r_p \\ 0 & 0 & 0 & 1 \end{bmatrix}. \quad (18)$$

According to [14], the linear and rotational velocities of the platform are as follows:

$$\vec{\omega}_Q = \begin{bmatrix} -s\theta_Q & 0 & 1 \\ s\varphi_Q c\theta_Q & c\varphi_Q & 0 \\ c\varphi_Q c\theta_Q & -s\varphi_Q & 0 \end{bmatrix} \begin{bmatrix} \dot{\psi}_Q \\ \dot{\theta}_Q \\ \dot{\phi}_Q \end{bmatrix},$$

$$\vec{v}_Q = \frac{d}{dt} G_Q, \quad G_Q = H_Q^O \begin{bmatrix} 0 \\ -d_{C_Q} \\ 0 \end{bmatrix}. \quad (19)$$

Furthermore, based on [14], for the actuator plane, we have:

$$BA : \vec{\omega}_{BA} = \begin{bmatrix} -s\theta_p & 0 & 1 \\ s\varphi_p c\theta_p & c\varphi_p & 0 \\ c\varphi_p c\theta_p & -s\varphi_p & 0 \end{bmatrix} \begin{bmatrix} \dot{\psi}_p \\ \dot{\theta}_p \\ \dot{\phi}_p \end{bmatrix}^T,$$

$$\vec{v}_{BA} = [\dot{x}_p \quad \dot{y}_p \quad \dot{z}_p]^T$$

$$RA_i : \vec{\omega}_{RA_i} = \vec{\omega}_{BA} + R_{RA_i}^O [0 \quad 0 \quad \dot{\beta}_i]^T,$$

$$\vec{v}_{RA_i} = \frac{d}{dt} G_{RA_i} \quad (20)$$

$$SA_i : \vec{\omega}_{SA_i} = \vec{\omega}_{RA_i}, \quad \vec{v}_{SA_i} = \frac{d}{dt} G_{SA_i},$$

$$\begin{cases} G_{RA_i} = H_{RA_i}^O [0 \quad 0 \quad d_{C_{RA}}]^T, \\ G_{SA_i} = H_{SA_i}^O [h_r \quad d_{C_{SA}} \quad 0]^T. \end{cases}$$

Table 2. Links D-H parameters

Link	e	γ	d	Θ
$PR A_1$	0	0	r_p	β_1

It should be noted that, due to the absence of relative rotation between the components RA_i and SA_i , the rotational velocities of the component RA_i are also valid for the component SA_i . The rotational velocity of each link consists of the same velocity of the actuator plane relative to the reference coordinates and the corresponding rotational velocity of the link and actuator plane. Furthermore, the linear velocities of all the components of the robot are equal to the derivative of the position of the center of mass of that component. So, we have:

$$\begin{aligned}
 L_{ui} : \quad \bar{\omega}_{L_{ui}} &= \bar{\omega}_{SA_i} + \mathbf{R}_{B_{ui}}^O [0 \quad 0 \quad \dot{\alpha}_{ui}]^T, \\
 \bar{v}_{L_{ui}} &= \frac{d}{dt} \mathbf{G}_{L_{ui}}, \\
 L_{di} : \quad \bar{\omega}_{L_{di}} &= \bar{\omega}_{SA_i} + \mathbf{R}_{B_{di}}^O [0 \quad 0 \quad \dot{\alpha}_{di}]^T, \\
 \bar{v}_{L_{di}} &= \frac{d}{dt} \mathbf{G}_{L_{di}}, \tag{21}
 \end{aligned}$$

$$\begin{cases} \mathbf{G}_{L_{ui}} = \mathbf{H}_{B_{ui}}^O d_{C_L} [-\sin(\alpha_{ui}) \quad \cos(\alpha_{ui}) \quad 0]^T \\ \mathbf{G}_{L_{di}} = \mathbf{H}_{B_{di}}^O d_{C_L} [-\sin(\alpha_{di}) \quad \cos(\alpha_{di}) \quad 0]^T \end{cases}$$

The kinetic and potential energies of the robot were calculated according to the [13]. Therefore, the platform energy is equal to:

$$\begin{cases} T_Q = \frac{1}{2} (\omega_Q^T \mathbf{I}_Q \omega_Q + m_Q \mathbf{v}_Q^T \mathbf{v}_Q) \\ U_Q = m_Q g \mathbf{G}_Q(2) \end{cases} \tag{22}$$

The link's energy is equal to:

$$\begin{cases} T_L = T_{L_u} + T_{L_d} \\ U_L = U_{L_u} + U_{L_d} \end{cases}, \\
 \begin{cases} T_{L_u} = \frac{1}{2} \sum_{i=1}^3 (\omega^T \mathbf{I} \omega + m \mathbf{v}^T \mathbf{v})_{L_{ui}} \\ T_{L_d} = \frac{1}{2} \sum_{i=1}^3 (\omega^T \mathbf{I} \omega + m \mathbf{v}^T \mathbf{v})_{L_{di}} \end{cases}, \tag{23} \\
 \begin{cases} U_{L_u} = \sum_{i=1}^3 (mg \mathbf{G}(2))_{L_{ui}} \\ U_{L_d} = \sum_{i=1}^3 (mg \mathbf{G}(2))_{L_{di}} \end{cases}.
 \end{cases}$$

The actuator's plane energies are equal to:

$$\begin{cases} T_P = T_{BA} + T_{RA} + T_{SA} \\ U_P = U_{BA} + U_{RA} + U_{SA} \end{cases}, \\
 \begin{cases} T_{BA} = \frac{1}{2} (\omega^T \mathbf{I} \omega + m \mathbf{v}^T \mathbf{v})_{BA} \\ T_{RA} = \frac{1}{2} \sum_{i=1}^3 (\omega^T \mathbf{I} \omega + m \mathbf{v}^T \mathbf{v})_{RA_i} \\ T_{SA} = \frac{1}{2} \sum_{i=1}^3 (\omega^T \mathbf{I} \omega + m \mathbf{v}^T \mathbf{v})_{SA_i} \end{cases} \tag{24} \\
 \begin{cases} U_{BA} = (mg \mathbf{G}(2))_{BA} \\ U_{RA} = \sum_{i=1}^3 (mg \mathbf{G}(2))_{RA_i} \\ U_{SA} = \sum_{i=1}^3 (mg \mathbf{G}(2))_{SA_i} \end{cases}.
 \end{cases}$$

where, g is the gravity acceleration. So, the total energy of the robot is equal to:

$$\begin{cases} T = T_Q + T_L + T_P \\ U = U_Q + U_L + U_P \end{cases} \tag{25}$$

According to [13] the equations of motion of the robot by the Euler-Lagrange method are as follows:

$$\frac{d}{dt} \left(\frac{\partial L}{\partial \dot{q}_i} \right) - \frac{\partial L}{\partial q_i} + \sum_{k=1}^{18} \lambda_k \frac{\partial f_k}{\partial q_i} = Q_i, \tag{26}$$

$$i = 1, 2, \dots, 24$$

in which, we have:

$$\begin{cases} L = T - U, \\ \mathbf{q} = \begin{bmatrix} x_Q, y_Q, z_Q, \psi_Q, \theta_Q, \varphi_Q, x_P, y_P, \\ z_P, \psi_P, \theta_P, \varphi_P, \alpha_{u1}, \alpha_{u2}, \alpha_{u3}, \\ \alpha_{d1}, \alpha_{d2}, \alpha_{d3}, \beta_1, \beta_2, \beta_3, b_1, b_2, b_3 \end{bmatrix} \\ \mathbf{Q} = \begin{bmatrix} 0, 0, 0, 0, 0, 0, 0, 0, 0, 0, 0, \\ 0, 0, 0, 0, 0, T_1, T_2, T_3, F_1, F_2, F_3 \end{bmatrix}^T. \end{cases} \tag{27}$$

and \mathbf{Q} represents the generalized forces, \mathbf{F}_i represents the force applied to the actuator i , in the direction of \mathbf{b}_i , and \mathbf{T}_i represents the torque applied to the actuator i , in the direction of β_i . In this study, the friction force of Columbus

was omitted. f_k is the relationship between the constraints obtained from Equation 9. So, based on [13] we have:

$$\left\{ \begin{aligned} \frac{d}{dt} \left(\frac{\partial L}{\partial \dot{q}_i} \right) &= \frac{d}{dt} \left(\frac{\partial(T-U)}{\partial \dot{q}_i} \right) = \frac{d}{dt} \left(\frac{\partial T}{\partial \dot{q}_i} \right) = \\ & \sum_{j=1}^n \frac{\partial}{\partial \dot{q}_j} \left(\frac{\partial T}{\partial \dot{q}_i} \right) \dot{q}_j + \sum_{j=1}^n \frac{\partial}{\partial q_j} \left(\frac{\partial T}{\partial \dot{q}_i} \right) \dot{q}_j, \\ \frac{\partial L}{\partial q_i} &= \frac{\partial(T-U)}{\partial q_i} = \frac{\partial T}{\partial q_i} - \frac{\partial U}{\partial q_i}, \\ \frac{\partial f_k}{\partial q_i} &= a_{ki}. \end{aligned} \right. \quad (28)$$

where we have:

$$\left\{ \begin{aligned} \frac{\partial}{\partial \dot{q}_j} \left(\frac{\partial T}{\partial \dot{q}_i} \right) &= m_{ij} \\ \frac{\partial U}{\partial q_i} &= g_i \\ s_{kj}(q, \dot{q}) &= \sum_{i=1}^n c_{kij}(q) \dot{q}_i \\ c_{kij}(q) &= \frac{1}{2} \left\{ \frac{\partial m_{kj}}{\partial q_i} + \frac{\partial m_{ki}}{\partial q_j} - \frac{\partial m_{ij}}{\partial q_k} \right\} \end{aligned} \right. \quad (29)$$

So, the equation of motion will be as follows:

$$\mathbf{M}(q)\ddot{\mathbf{q}} + \mathbf{S}(q, \dot{\mathbf{q}})\dot{\mathbf{q}} + \mathbf{G}(q) + \mathbf{A}^T \boldsymbol{\lambda} = \mathbf{Q} \quad (30)$$

where \mathbf{M} is the mass and inertia matrix. \mathbf{S} is the Coriolis matrix, \mathbf{G} is the gravity vector, \mathbf{A} is the weight matrix of Lagrangian coefficients, and \mathbf{Q} is the generalized force vector. \mathbf{M} is a positive-definite and symmetric inertia matrix. The elements of this matrix are bounded since unboundedness results in singularity and show the region that is not within the workspace of the robot. Furthermore, $\dot{\mathbf{M}} - 2\mathbf{S}$ is skew-symmetric. Eq. (32) is sufficient for inverse dynamic modeling, but for direct dynamic modeling, the state-space equation is required. For this purpose, we need to eliminate the Lagrange coefficients from the equation of motion. In this regard, the null matrix \mathbf{A} was obtained using Eq. (12) and the following definition [15]:

$$\left\{ \begin{aligned} \ddot{\mathbf{q}} &= \begin{bmatrix} \dot{\mathbf{X}}_p^T & \dot{\mathbf{X}}_a^T \end{bmatrix}^T = \mathbf{N}\ddot{\mathbf{X}}_a \\ \ddot{\mathbf{q}} &= \dot{\mathbf{N}}\dot{\mathbf{X}}_a + \mathbf{N}\ddot{\mathbf{X}}_a \quad \rightarrow \quad \mathbf{AN} = 0 \\ \mathbf{N}_{24 \times 6} &= \begin{bmatrix} \mathbf{J} \\ \mathbf{I}_{6 \times 6} \end{bmatrix} \end{aligned} \right. \quad (31)$$

where \mathbf{N} is the null matrix of \mathbf{A} . To calculate the derivative of the null matrix, we can write:

$$\left\{ \begin{aligned} \mathbf{AN} = 0 &\rightarrow \dot{\mathbf{A}}\mathbf{N} + \mathbf{A}\dot{\mathbf{N}} = 0 \rightarrow \\ \dot{\mathbf{N}} &= -\mathbf{A}^{-1}\dot{\mathbf{A}}\mathbf{N} \\ \mathbf{A}^{-1} &= \mathbf{A}^T (\mathbf{AA}^T)^{-1} \end{aligned} \right. \quad (32)$$

Multiplying \mathbf{N}^T from the left in Eq. (30) and placing the derivatives \mathbf{q} , we have:

$$\mathbf{N}^T \mathbf{M} (\dot{\mathbf{N}}\dot{\mathbf{X}}_a + \mathbf{N}\ddot{\mathbf{X}}_a) + \mathbf{N}^T \mathbf{S} \mathbf{N} \dot{\mathbf{X}}_a + \mathbf{N}^T \mathbf{G} = \bar{\mathbf{F}} \quad (33)$$

where $\mathbf{N}^T \mathbf{Q} = \bar{\mathbf{F}} = [T_1 \quad T_2 \quad T_3 \quad F_1 \quad F_2 \quad F_3]^T$. So, Eq. (30) can be rewritten as follows:

$$\left\{ \begin{aligned} \tilde{\mathbf{M}}_{6 \times 6} &= \mathbf{N}^T \mathbf{M} \mathbf{N} \\ \tilde{\mathbf{S}}_{6 \times 6} &= (\mathbf{N}^T \dot{\mathbf{M}} \mathbf{N} + \mathbf{N}^T \mathbf{S} \mathbf{N}) \rightarrow \\ \tilde{\mathbf{G}}_{6 \times 1} &= \mathbf{N}^T \mathbf{G} \end{aligned} \right. \quad (34)$$

$$\tilde{\mathbf{M}}\ddot{\mathbf{X}}_a + \tilde{\mathbf{S}}\dot{\mathbf{X}}_a + \tilde{\mathbf{G}} = \bar{\mathbf{F}}$$

It can also be written:

$$a. \tilde{\mathbf{M}}^T = (\mathbf{N}^T \mathbf{M} \mathbf{N})^T = \mathbf{N}^T \mathbf{M}^T \mathbf{N} = \mathbf{N}^T \mathbf{M} \mathbf{N} = \tilde{\mathbf{M}}$$

$$b. \begin{aligned} \dot{\tilde{\mathbf{M}}} - 2\tilde{\mathbf{S}} &= 2\mathbf{N}^T \dot{\mathbf{M}} \mathbf{N} + \mathbf{N}^T \dot{\mathbf{M}} \mathbf{N} \\ &\quad - 2(\mathbf{N}^T \dot{\mathbf{M}} \mathbf{N} + \mathbf{N}^T \mathbf{S} \mathbf{N}) \rightarrow \\ \dot{\tilde{\mathbf{M}}} - 2\tilde{\mathbf{S}} &= \mathbf{N}^T \dot{\mathbf{M}} \mathbf{N} - 2\mathbf{N}^T \mathbf{S} \mathbf{N} = \\ &\quad \mathbf{N}^T (\dot{\mathbf{M}} - 2\mathbf{S}) \mathbf{N} \rightarrow \\ (\dot{\tilde{\mathbf{M}}} - 2\tilde{\mathbf{S}})^T &= (\mathbf{N}^T (\dot{\mathbf{M}} - 2\mathbf{S}) \mathbf{N})^T = \\ &\quad \mathbf{N}^T (\dot{\mathbf{M}} - 2\mathbf{S})^T \mathbf{N} = \\ &\quad -\mathbf{N}^T (\dot{\mathbf{M}} - 2\mathbf{S}) \mathbf{N} = -(\dot{\tilde{\mathbf{M}}} - 2\tilde{\mathbf{S}}) \end{aligned} \quad (35)$$

So $\tilde{\mathbf{M}}$ is symmetric and $\dot{\tilde{\mathbf{M}}} - 2\tilde{\mathbf{S}}$ is also skew-symmetric. By selecting the state variables in the form $\bar{\mathbf{X}}_{12 \times 1} = [\bar{\mathbf{X}}_a^T, \dot{\bar{\mathbf{X}}}_a^T]^T$, the system state space is:

$$\begin{aligned} \dot{\bar{\mathbf{X}}} &= \begin{bmatrix} \dot{\bar{\mathbf{X}}}_a \\ \ddot{\bar{\mathbf{X}}}_a \end{bmatrix} = \begin{bmatrix} \dot{\bar{\mathbf{X}}}_a \\ \mathbf{W} \end{bmatrix} + \begin{bmatrix} [0]_{6 \times 6} \\ \tilde{\mathbf{M}}^{-1} \end{bmatrix} \bar{\mathbf{F}} \\ \mathbf{W} &= -\tilde{\mathbf{M}}^{-1} (\tilde{\mathbf{S}}\dot{\bar{\mathbf{X}}}_a + \tilde{\mathbf{G}}) \end{aligned} \quad (36)$$

2- 2- 2- Virtual Work Method

In order to model using the virtual work method, the forces, and torques applied to the center of mass of the robot parts were calculated as follows [16]:

$$\begin{aligned}
 \mathbf{F}_Q &= \begin{bmatrix} Force \\ Torque \end{bmatrix}_Q = \begin{bmatrix} \mathbf{F}_e \\ \mathbf{T}_e \end{bmatrix} + \begin{bmatrix} mg - m\dot{\mathbf{v}} \\ -\mathbf{I}\dot{\boldsymbol{\omega}} - \boldsymbol{\omega} \times (\mathbf{I}\boldsymbol{\omega}) \end{bmatrix}_Q, \\
 \mathbf{F}_{BA} &= \begin{bmatrix} mg - m\dot{\mathbf{v}} \\ -\mathbf{I}\dot{\boldsymbol{\omega}} - \boldsymbol{\omega} \times (\mathbf{I}\boldsymbol{\omega}) \end{bmatrix}_{BA}, \\
 \mathbf{F}_{L_{ui}} &= \begin{bmatrix} mg - m\dot{\mathbf{v}} \\ -\mathbf{I}\dot{\boldsymbol{\omega}} - \boldsymbol{\omega} \times (\mathbf{I}\boldsymbol{\omega}) \end{bmatrix}_{L_{ui}}, \\
 \mathbf{F}_{L_{di}} &= \begin{bmatrix} mg - m\dot{\mathbf{v}} \\ -\mathbf{I}\dot{\boldsymbol{\omega}} - \boldsymbol{\omega} \times (\mathbf{I}\boldsymbol{\omega}) \end{bmatrix}_{L_{di}}.
 \end{aligned} \tag{37}$$

$$\delta \begin{bmatrix} \mathbf{q}_Q \\ \mathbf{q}_{BA} \\ \mathbf{q}_{L_u} \\ \mathbf{q}_{L_d} \end{bmatrix} = \mathbf{J} \delta \begin{bmatrix} \mathbf{q}_{RA} \\ \mathbf{q}_{SA} \end{bmatrix}$$

Now, by rewriting Eq. (38) in the matrix form and using Eq. (39), we have:

Using the principle of virtual work, we have:

$$\begin{aligned}
 &\delta \mathbf{q}_Q^T \mathbf{F}_Q + \delta \mathbf{q}_{BA}^T \mathbf{F}_{BA} + \\
 &\sum_{i=1}^3 (\delta \mathbf{q}_{RA_i}^T \mathbf{T}_i + \mathbf{q} \mathbf{x}_{SA_i}^T \mathbf{F}_i + \mathbf{q} \mathbf{x}_{L_{ui}}^T \mathbf{F}_{L_{ui}} + \mathbf{q} \mathbf{x}_{L_{di}}^T \mathbf{F}_{L_{di}}) = 0 \tag{38}
 \end{aligned}$$

The virtual displacements in Eq. (38) must be consistent with the kinematic constraints imposed by the links. Therefore, it is necessary to relate the above virtual displacements to a set of independent generalized virtual displacements. So, using Eq. (12), we have:

$$\begin{aligned}
 \mathbf{q}_Q &= [x_Q, y_Q, z_Q, \psi_Q, \theta_Q, \varphi_Q]^T \\
 \mathbf{q}_{BA} &= [x_P, y_P, z_P, \psi_P, \theta_P, \varphi_P]^T \\
 \mathbf{q}_{RA_i} &= \beta_i, \quad \mathbf{q}_{SA_i} = b_i, \quad \mathbf{q}_{L_{ui}} = \alpha_{ui}, \quad \mathbf{q}_{L_{di}} = \alpha_{di}
 \end{aligned} \tag{39}$$

$$\begin{aligned}
 &[\delta \mathbf{q}_Q^T, \delta \mathbf{q}_{BA}^T, \delta \mathbf{q}_{L_u}^T, \delta \mathbf{q}_{L_d}^T] \begin{bmatrix} \mathbf{F}_Q \\ \mathbf{F}_{BA} \\ \mathbf{F}_{L_u} \\ \mathbf{F}_{L_d} \end{bmatrix} + \\
 &[\delta \mathbf{q}_{RA}^T, \delta \mathbf{q}_{SA}^T] \begin{bmatrix} \mathbf{T} \\ \mathbf{F} \end{bmatrix} = 0 \rightarrow \\
 &[\delta \mathbf{q}_{RA}^T, \delta \mathbf{q}_{SA}^T] \mathbf{J}^T \begin{bmatrix} \mathbf{F}_Q \\ \mathbf{F}_{BA} \\ \mathbf{F}_{L_u} \\ \mathbf{F}_{L_d} \end{bmatrix} + [\delta \mathbf{q}_{RA}^T, \delta \mathbf{q}_{SA}^T] \begin{bmatrix} \mathbf{T} \\ \mathbf{F} \end{bmatrix} = 0 \tag{40} \\
 &\rightarrow \begin{bmatrix} \mathbf{T} \\ \mathbf{F} \end{bmatrix} = -\mathbf{J}^T \begin{bmatrix} \mathbf{F}_Q \\ \mathbf{F}_{BA} \\ \mathbf{F}_{L_u} \\ \mathbf{F}_{L_d} \end{bmatrix}
 \end{aligned}$$

Table 3. Simulation parameter values

	Mark	unit	value
moving plane radius	r_Q	(m)	0.24
base plane radius	r_O	(m)	0.24
above links length	l_u	(m)	0.33
lower links length	l_d	(m)	0.33
distance of the actuator plane to the center of the prismatic joint	h_r	(m)	0.03
distance of the base plane to the center of the spherical joint	h_s	(m)	0.03
moving plane mass	m_Q	(kg)	1.63
mass of the above links	m_u	(kg)	0.88
mass of the lower links	m_d	(kg)	0.88
actuator plane mass	m_{BA}	(kg)	0.09
mass of revolute actuator set	m_{RA}	(kg)	0.12
mass of prismatic actuator set	m_{SA}	(kg)	0.56
gravity acceleration	g	(m/s ²)	9.8

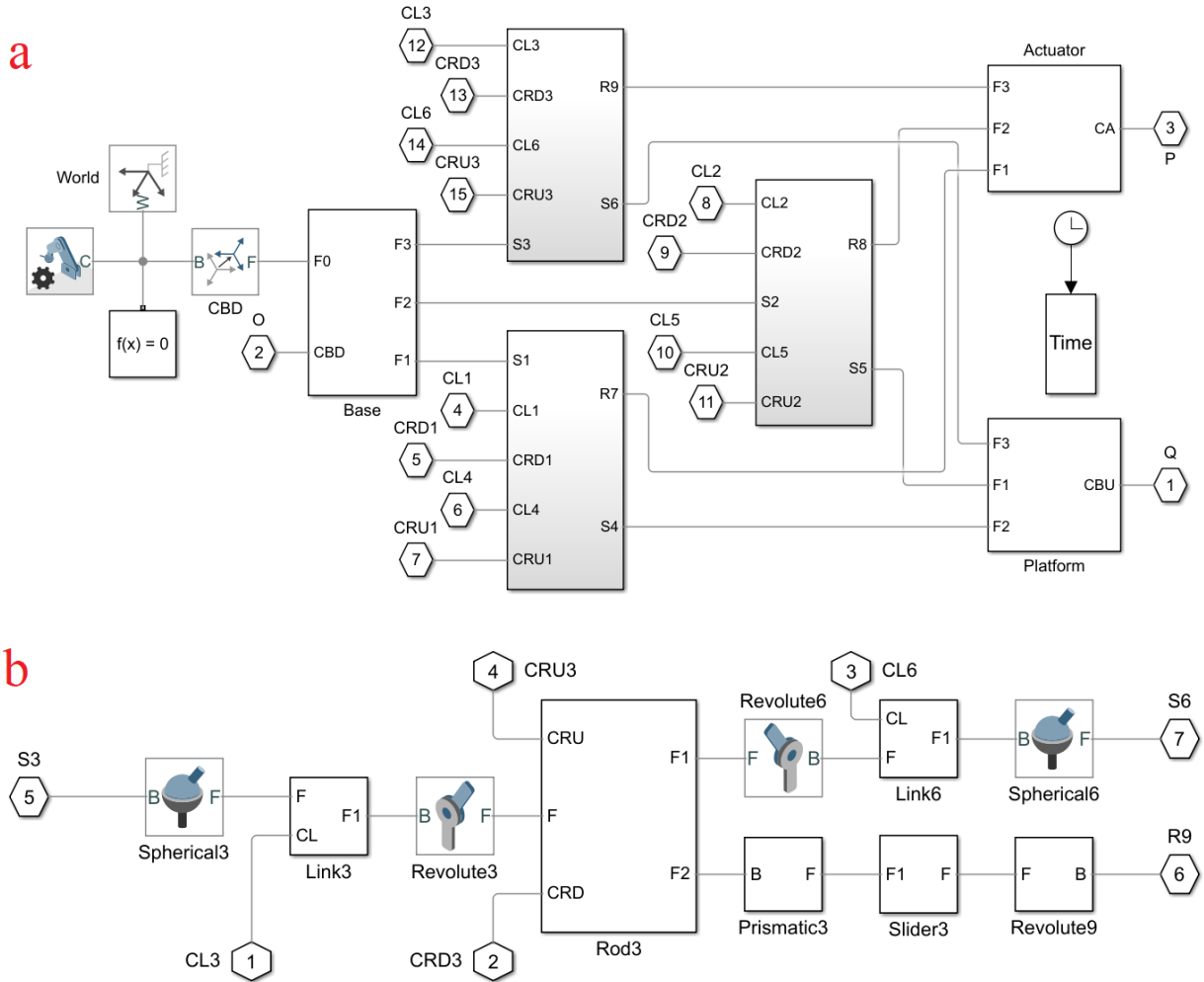


Fig. 6. SimScape model of the CT-3RPRS robot: (a: main model, b: subsystem)

The final form of Eq. (40) will represent the inverse dynamic equation of the CT-3RPRS robot.

3- Simulation study

Simulation parameter values are listed in Table 3:

3- 1- Model verification:

In this section, modeling of the CT-3RPRS robot is performed using the SimScape environment of MATLAB software (The MathWorks, Inc. Natick, MA). By using this model, verifying the mathematical model is performed. CT-3RPRS robot SimScape model is shown in Fig. 6.

One of the most significant sources of error in modeling arises from the inaccurate application of small-scale velocities within the dynamic equations. To evaluate the effectiveness of the proposed dynamic model, the accuracy of its performance is assessed by examining relatively rapid changes over a short time interval. This approach allows for a precise measurement of the model’s capability to capture dynamic behaviors under transient conditions. To verify the

dynamics modeling, the selected paths of the actuators given in Eq. (41) were used as input to the SimScape model; and the forces and torques generated in the prismatic and revolute joints were measured; and compared with the forces and torques calculated by simulation in MATLAB environment using virtual work method.

$$\begin{aligned}
 \begin{bmatrix} \beta_1 \\ \beta_2 \\ \beta_3 \end{bmatrix} &= \frac{\pi}{10} \sin(2t) \begin{bmatrix} 1 \\ 1 \\ 1 \end{bmatrix}, \\
 \begin{bmatrix} b_1 \\ b_2 \\ b_3 \end{bmatrix} &= 0.35 + 0.01 \begin{bmatrix} -4\sin(0.5t) \\ -5\sin(t) \\ 4.5\sin(2t) \end{bmatrix}
 \end{aligned} \tag{41}$$

The results of this analogy are shown in Fig. 7

Fig. 7 illustrates the comparison of forces and torques obtained from two different simulation approaches: MATLAB (using the virtual work method) and SimScape. The forces

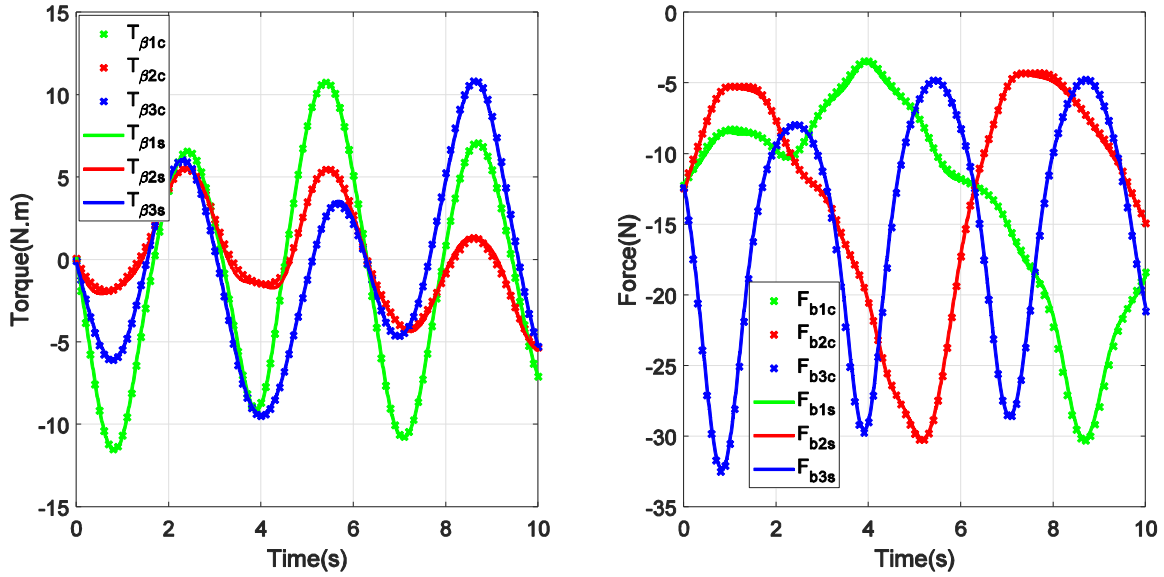


Fig. 7. Forces and torques calculated with MATLAB (c) and SimScape (S).

and torques are plotted over a time range of 0 to 10 seconds. The results demonstrate a high degree of compatibility between the two methods, indicating the accuracy of the dynamic model derived using the virtual work method. The slight discrepancies observed can be attributed to differences in numerical precision and the estimation techniques used in MATLAB and SimScape environments.

Fig. 8 presents the percentage error between the forces and torques calculated using MATLAB (virtual work method) and SimScape. The error remains within an acceptable range of approximately 1%, which validates the consistency of the dynamic model. The minor errors are likely due to the inherent differences in the numerical solvers and the precision of inertial matrix calculations in the two software environments. This figure reinforces the reliability of the proposed dynamic modeling approach.

3- 2- Forward and inverse dynamics

To simulate forward and inverse dynamics, the inverse dynamics of the system (extracted using the virtual work method) were modeled using the path in Eq. (42); and the generalized forces of the robot were extracted. Then, forward dynamics were simulated using these generalized forces and the Euler-Lagrange method. Active and passive positions were extracted and compared with the expected values.

$$\begin{bmatrix} \beta_1 \\ \beta_2 \\ \beta_3 \end{bmatrix} = \frac{\pi}{10} \sin(2t) \begin{bmatrix} 1 \\ 1 \\ 1 \end{bmatrix}, \tag{42}$$

$$\begin{bmatrix} b_1 \\ b_2 \\ b_3 \end{bmatrix} = 0.39132 + 0.02 \begin{bmatrix} -4\sin(0.5t) \\ -5\sin(t) \\ 4.5\sin(2t) \end{bmatrix}$$

A summary of the performed process is shown in Fig. 9:

A comparison of desired and forward dynamics trajectory of planes Q, P, and link angles in Figs. 10 and 11 are performed.

Fig. 10 compares the desired trajectories of the link angles with those obtained from the forward dynamics simulation using the Euler-Lagrange method. The close alignment between the desired and simulated trajectories confirms the accuracy of the forward dynamics model. This comparison is crucial for validating the mathematical formulation of the robot's dynamics, as it ensures that the simulated behavior matches the expected physical response.

Fig. 11 shows the comparison between the desired trajectories of planes Q and P and the trajectories generated by the forward dynamics simulation. The results indicate a strong agreement between the desired and simulated trajectories, further validating the accuracy of the dynamic model. This figure highlights the effectiveness of the Euler-Lagrange method in predicting the robot's motion in different planes.

Fig. 12 displays the actuator forces and torques obtained from the inverse dynamics simulation using the virtual work method. The smooth and continuous nature of the forces and torques, without any abrupt changes or discontinuities, indicates the robustness and accuracy of the inverse dynamics model. This smoothness is essential for ensuring stable and reliable control of the robot's actuators in practical applications.

4- Conclusion

This study successfully developed a comprehensive dynamic model of the novel parallel spatial robot CT-3RPRS, utilizing both the Euler-Lagrange and virtual work methods. The model encompassed both kinematic and kinetic aspects of the robot, providing a complete representation of its

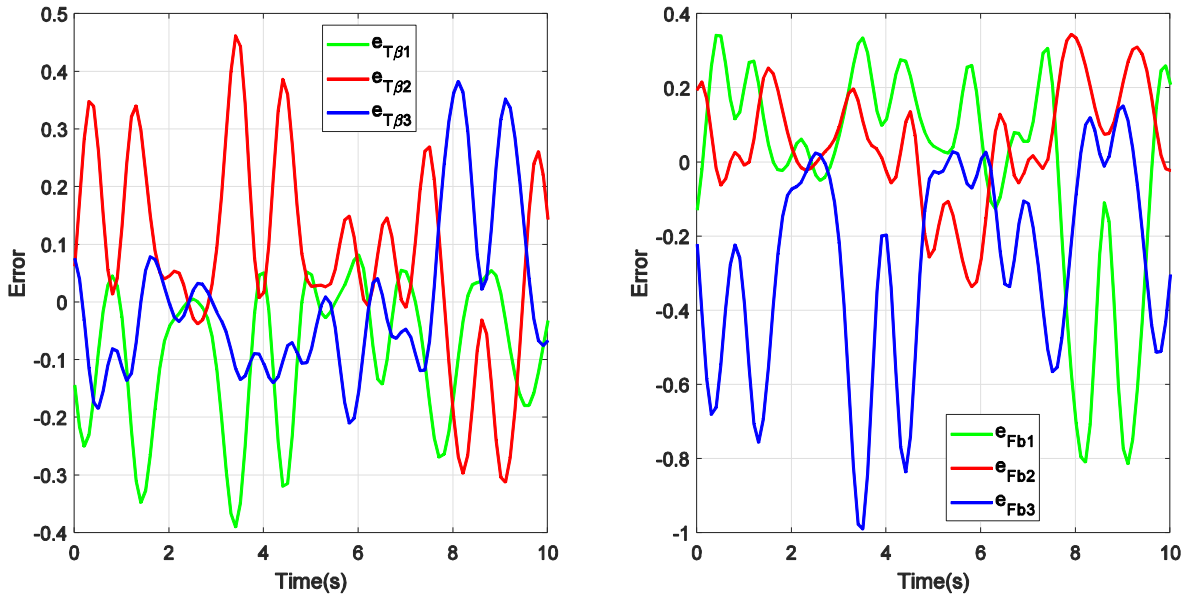


Fig. 8. Forces and torques errors (%) between MATLAB and SimScape.

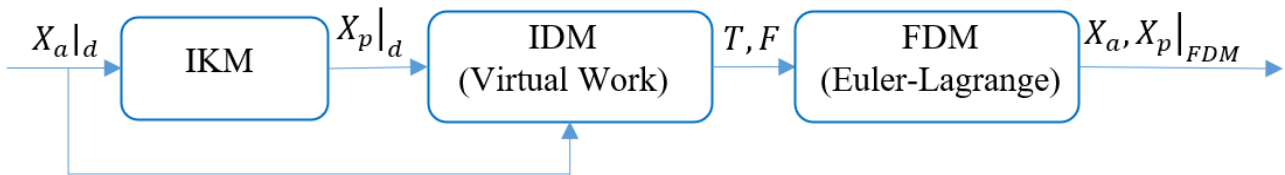


Fig. 9. A schematic of the simulation processes

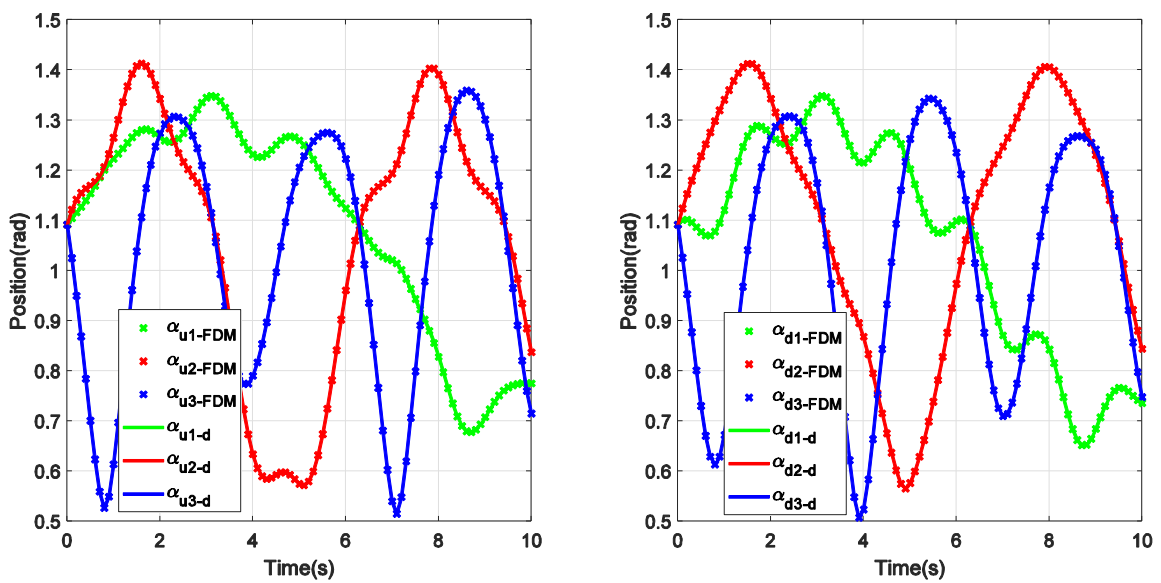


Fig. 10. Comparison of desired (d) and forward dynamics (FDM) trajectory of link angles

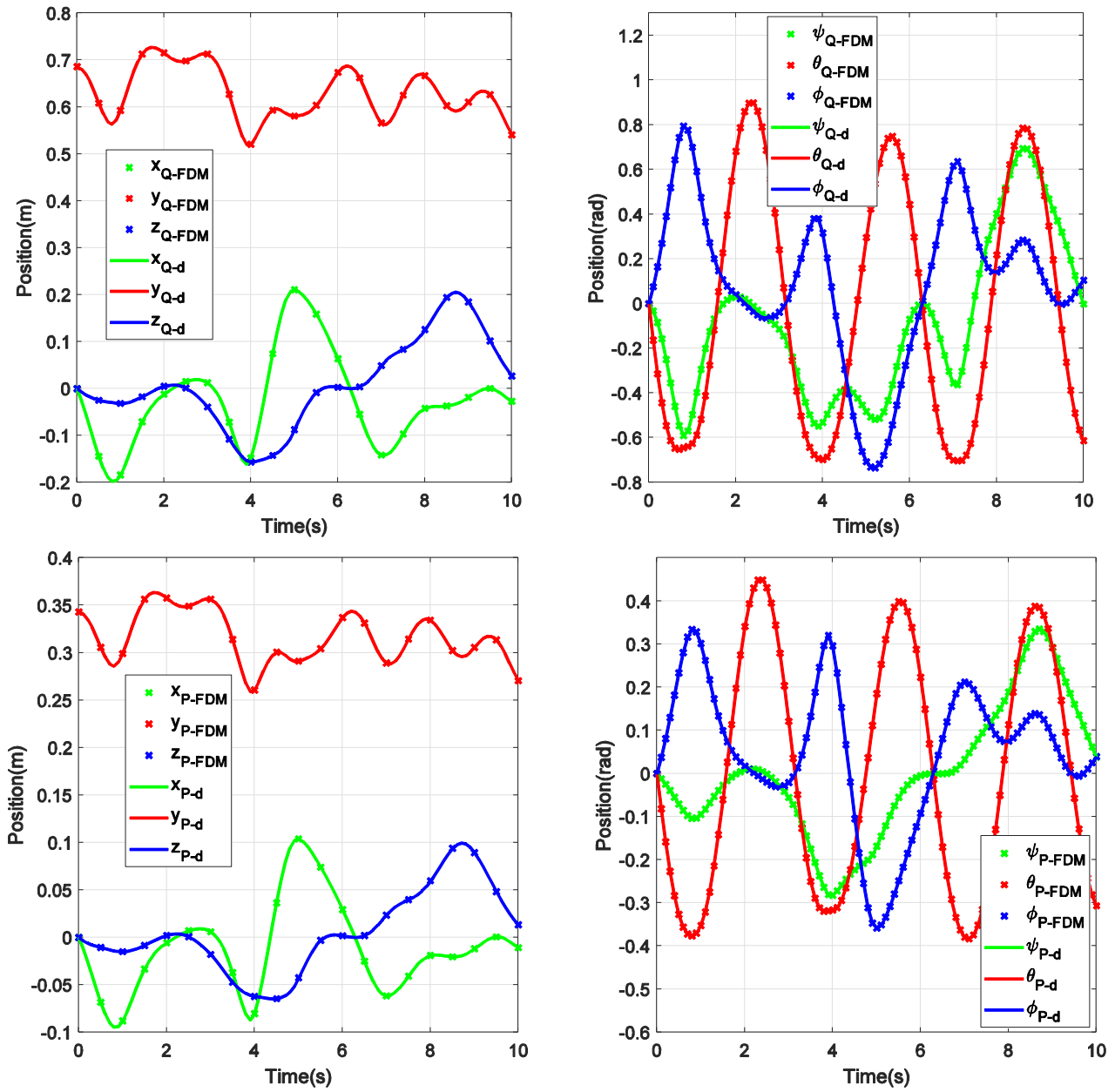


Fig. 11. Comparison of desired (d) and forward dynamics (FDM) trajectory of planes Q, P.

behavior. Lagrange multipliers were employed to derive dynamic equations for the constrained system, ensuring accurate modeling of the robot's movement. Rigorous validation was achieved through analytical and comparative simulation scenarios within MATLAB, further corroborated by verification with SimScape. The results demonstrated excellent compatibility between the MATLAB and SimScape models, with a negligible error of less than 3% observed in

the dynamic simulation. Moreover, the dynamic equations were simulated and compared in direct and inverse scenarios, revealing strong consistency between the Euler-Lagrange and virtual work methods. This robust and validated model provides a valuable foundation for future research on control, optimization, and trajectory planning for the CT-3RPRS robot, contributing to its potential applications in various industrial and robotic domains.

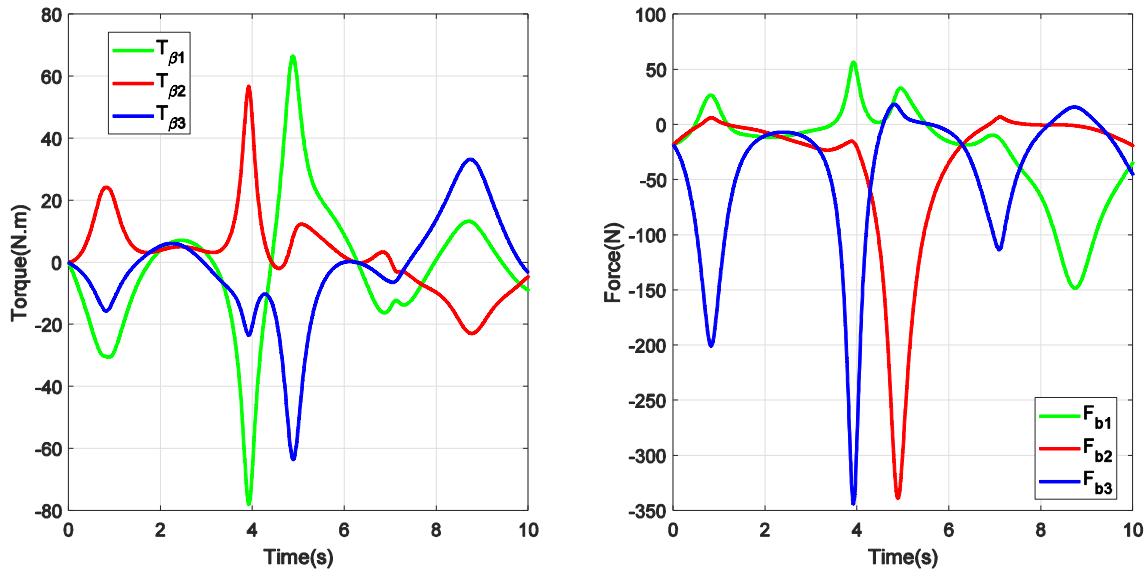


Fig. 12. Actuator forces and torques from inverse dynamics simulations

Nomenclature

r	Radius, m
l	Links length, m
h	joint length, m
m	mass, Kg
g	Gravity acceleration, m/s ²

Greek symbols

α	Link angle, rad
β	Revolute joint angle, rad
ψ	yaw angle, rad
θ	pitch angle, rad
φ	roll angle, rad

Subscript

o	Global coordinates origin
p	Actuator plane coordinates origin
q	End-effector coordinates origin
s	Spherical joint
u	upper part of the revolute joint
d	down of the revolute joint
a	active generalized coordinate
p	passive generalized coordinate
L	Links of robot
i	Number of each parameter

References

- [1] J.-P. Merlet, Parallel robots, Springer Science & Business Media, Dordrecht, Netherlands, 2006.
- [2] O. Gholami, B. Miripour Fard, Enhanced workspace through the conjoined twins modification of the Stewart platform, Mechanics Based Design of Structures and Machines, (2024) 1-13.
- [3] O. Gholami, B. Miripour Fard, Conjoined twins 3RPRS: a novel parallel spatial robot, Mechanics Based Design of Structures and Machines, 52(5) (2024) 2821-2840.
- [4] S.P.S. Kumar, S. Bandyopadhyay, Forward kinematics of the 3-RPRS parallel manipulator using a geometric approach, in: Machines, Mechanism and Robotics, Springer, 2019, pp. 159-169.
- [5] A. Nag, S. Mohan, S. Bandyopadhyay, Forward kinematic analysis of the 3-RPRS parallel manipulator, Mechanism and Machine Theory, 116 (2017) 262-272.
- [6] H. Simas, A. Dias, D. Martins, Kinematic Model for Eclipse and Eclipse-II Parallel Robot, in: ABCM Symposium Series in Mechatronics, 2009, pp. 719-728.
- [7] V. Venkatesan, Y. Singh, S. Mohan, Inverse kinematic solution of a 6-DOF (3-RPRS) parallel spatial manipulator, in: Proceedings of the 3rd Joint International Conference on Multibody System, 2014.
- [8] S. Mohan, B. Corves, Inverse dynamics and trajectory tracking control of a new six degrees of freedom spatial 3-RPRS parallel manipulator, Mechanical Sciences, 8(2) (2017) 235.
- [9] Y. Li, Q. Xu, Kinematics and inverse dynamics analysis for a general 3-PRS spatial parallel mechanism, Robotica, 23(02) (2005) 219-229.
- [10] G. Pond, J.A. Carretero, Architecture optimisation of three 3-RS variants for parallel kinematic machining,

- Robotics and Computer-Integrated Manufacturing, 25(1) (2009) 64-72.
- [11] S. Staicu, Matrix modeling of inverse dynamics of spatial and planar parallel robots, *Multibody System Dynamics*, 27(2) (2012) 239-265.
- [12] H. Tourajizadeh, O. Gholami, CLOSED LOOP NONLINEAR OPTIMAL CONTROL OF A 3PRS PARALLEL ROBOT, *International Journal of Robotics and Automation*, 36(2) (2021).
- [13] R.N. Jazar, *Advanced dynamics: rigid body, multibody, and aerospace applications*, John Wiley & Sons, 2011.
- [14] H. Baruh, *Analytical dynamics*, (No Title), (1999).
- [15] C. Liang, G.M. Lance, A differentiable null space method for constrained dynamic analysis, *Journal of Mechanisms, Transmissions, and Automation in Design*, 109(3) (1987) 405-411.
- [16] L.-W. Tsai, Solving the inverse dynamics of a Stewart-Gough manipulator by the principle of virtual work, *J. Mech. Des.*, 122(1) (2000) 3-9.

HOW TO CITE THIS ARTICLE

O. Gholami, B. Miripour Fard, *Exploring the Kinematics and Kinetics of the novel CT-3RPRS Robot*, *AUT J. Mech Eng.*, 9(3) (2025) 265-280.

DOI: [10.22060/ajme.2025.23647.6148](https://doi.org/10.22060/ajme.2025.23647.6148)

